



Simple and compact grating-based heterodyne interferometer with the Littrow configuration for high-accuracy and long-range measurement of two-dimensional displacement

QIANG LV,^{1,2} ZHAOWU LIU,¹  WEI WANG,^{1,3} XIAOTIAN LI,¹ SHUO LI,¹ YING SONG,¹ HONGZHU YU,¹ BAYANHESHIG,¹ AND WENHAO LI^{1,*}

¹Changchun Institute of Optics, Fine Mechanics and Physics, Chinese Academy of Sciences, Changchun, Jilin 130033, China

²University of Chinese Academy of Sciences, Beijing 100049, China

³e-mail: wayne_lzu@163.com

*Corresponding author: liwh@ciomp.ac.cn

Received 24 July 2018; revised 8 October 2018; accepted 8 October 2018; posted 10 October 2018 (Doc. ID 340587); published 30 October 2018

We propose a simple and compact reading head with the Littrow configuration that will increase measurement range and reduce the complexity of a two-dimensional grating-based interferometer. The reading head contains only a beam splitter, two polarizing beam splitter modules, and two mirrors. The theoretical resolutions in two directions are 0.27 nm and 0.18 nm, respectively. In comparison with a dual-frequency laser interferometer, the proposed interferometer can measure displacement from 3 nm to 10 mm with high accuracy. The 3σ values in two directions for the difference are 1.67 nm and 1.35 nm for a displacement of 9 nm. Repeatability for a displacement of 1 μm is better than 2 nm. © 2018 Optical Society of America

<https://doi.org/10.1364/AO.57.009455>

1. INTRODUCTION

Precision displacement measurement technology plays a very important role in semiconductor manufacturing, precision machining, microscopic techniques, photolithography, and other fields [1–5]. Laser interferometry [6,7] and grating-based interferometry [8] are the main techniques used to achieve a large measurement range and high measurement accuracy. However, the laser interferometer always suffers from errors and noise, most likely resulting from variations in temperature, air humidity, and carbon dioxide concentration [9]. In contrast, the grating-based interferometer is less affected by the environment because the structure of the reading head is symmetrical and the optical path is short [10], and this has become one of the most important factors in the rapid development of grating-based interferometry.

At present, most grating-based interferometers can measure displacement in only one dimension. Generally, a one-dimensional grating is used to measure displacement in the vector direction of the grating, but a grating-based interferometer that can measure multi-dimensional displacement with high accuracy is preferable. The two-dimensional grating is usually used to measure displacement in two dimensions (in the two vector directions of the two-dimensional grating) [11–13]. Due to limitations on the size of the two-dimensional grating, the

measurement range of the two-dimensional grating-based interferometer is very small. To measure displacement in a direction normal to the grating, a reference grating or a reference mirror must be introduced to the system [14–17]. This increases the complexity of the system, and the measurement range normal to the grating is limited by the size of the detectors and optical elements in the reading head. Although Guan *et al.* [18] measured displacement in a direction normal to the grating without a reference arm, the measurement range was still limited by the size of the detector. Agilent Technologies has put forward some proposals in patent [19] that use a one-dimensional grating to measure two-dimensional displacement in the Littrow configuration. With this method, the measurement range of the system in two directions is limited only by the length of the one-dimensional grating, which is helpful in enlarging the measurement range. However, the structure of the reading head has no integrated design, and no experiments or analyses have been reported to test the performance of the system. Lu *et al.* [20] verified the performance of the system designed using this method and analyzed the cosine error of the system. However, the structure of the system is too complex. The complex structure makes installation and debugging more difficult, which is not good for improving the accuracy of the system. It also restricts the application scope of the system, and this makes it more difficult to expand the

system for three-dimensional measurements. Šiaudinytė *et al.* [21] proposed a grating interferometer with the Littrow configuration containing a commercially available, minimized Michelson interferometer and three fiber-fed measurement heads. The diameter of the reading head is only 4 mm, which is smaller than many commercially available encoder heads. The system uses a grating with a period of 8 μm, and the measurement range is up to 450 mm. However, the resolution and accuracy of the system are low due to the use of a homodyne and grating with low line density, and installation of the system is difficult due to the small incident angle. Therefore, it becomes necessary to design a simple and compact grating-based interferometer with high accuracy and resolution, and the characteristics of convenient installation and wide application.

In this paper, we describe a reading head for a two-dimensional grating-based interferometer using the Littrow configuration that has the advantages of small size, simple structure, high accuracy, and high resolution. The reading head and a one-dimensional grating with a grating period of 555.6 nm and electronic subdivision of 1024 make up the two-dimensional grating-based interferometer. Our experiments demonstrated that, compared with the laser interferometer, the system has the ability to measure displacement in two directions with high accuracy and long range. It also has good repeatability and stability. We analyzed the measurement errors caused by the yaw angle, which significantly affects the accuracy of the system. Because of the simple structure of the reading head, the scope of application of the system is wider. It is easier to expand the system to measure three-dimensional displacements, which is very important for precise measurement of displacement.

2. MEASUREMENT PRINCIPLE

Figure 1 illustrates the optical configuration of our proposed grating-based interferometer. For convenience, the z axis is selected to be in the direction normal to the grating, and the x axis is in the vector direction of the grating. The grating-based interferometer consists of main five parts: a dual-frequency laser, a reading head, a grating, two receivers (R_1 and R_2), and a signal processing system. The reading head includes a beam splitter (BS), two polarizing beam splitters (PBS_1 and PBS_2), four quarter-wave plates ($QW_1 - QW_4$), and four mirrors ($M_1 - M_4$). The orthogonal linear polarized beam emitted by the dual-frequency laser at a certain beat frequency is split into two beams by the BS. One beam is incident to PBS_1 and the other is incident to PBS_2 . PBS_1 (PBS_2) reflects the

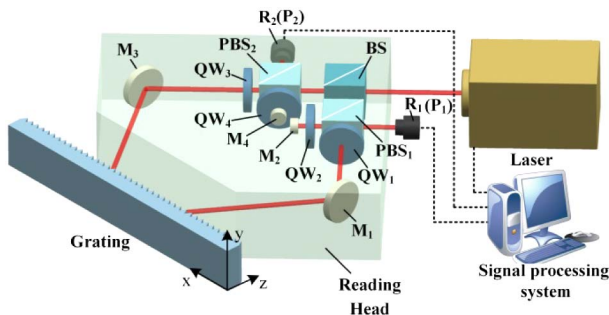


Fig. 1. System configuration for 2D displacement measurement.

s -polarized reference beam. The direction of polarization is changed by 90° after passing through QW_2 (QW_4), M_2 (M_4), and QW_2 (QW_4). The beam is then transmitted through PBS_1 (PBS_2) and enters R_1 (R_2). PBS_1 (PBS_2) transmits the p -polarized measurement beam, which then passes through QW_1 (QW_3) and is incident on the grating at the Littrow angle after being reflected by M_1 (M_3). The diffracted light is returned along the original path. The direction of polarization of the measurement beam is changed by 90° through M_1 (M_3) and QW_1 (QW_3) and is then reflected by PBS_1 (PBS_2) and also enters R_1 (R_2). There is a polarizer P_1 (P_2) in R_1 (R_2). The transmission axis of polarizer P_1 (P_2) is 45 deg to the polarization direction of incident light. After passing through the polarizers in the receivers, the measurement and reference beams interfere in the detector. For convenience, the propagation paths of the beams are given as follows:

Measurement beam 1: Laser - BS - PBS_1 - QW_1 - M_1 - Grating - M_1 - QW_1 - PBS_1 - P_1 - R_1

Reference beam 1: Laser - BS - PBS_1 - QW_2 - M_2 - QW_2 - PBS_1 - P_1 - R_1

Measurement beam 2: Laser - BS - PBS_2 - QW_3 - M_3 - Grating - M_3 - QW_3 - PBS_2 - P_2 - R_2

Reference beam 2: Laser - BS - PBS_2 - QW_4 - M_4 - QW_4 - PBS_2 - P_2 - R_2

The following is the principle of displacement measurement.

The complex amplitude of the orthogonal linear polarized beam emitted by the dual-frequency laser at a certain beat frequency is

$$E = E_0 \begin{pmatrix} e^{i(-2\pi f_1 t + \varphi_0)} \\ e^{i(-2\pi f_2 t + \varphi'_0)} \end{pmatrix}, \quad (1)$$

where f_1 and f_2 are the frequencies of the orthogonal linear polarized beam, φ_0 and φ'_0 are the initial phases and they are constants, and E_0 is the amplitude.

When the beams pass through the optical elements and enter the receivers, the electrical fields of measurement beams and reference beams are

$$\begin{cases} E_{m1} \propto E_0 e^{i(-2\pi f_1 t + \varphi_0 + \phi_1)} \\ E_{r1} \propto E_0 e^{i(-2\pi f_2 t + \varphi'_0)} \end{cases}, \quad (2)$$

$$\begin{cases} E_{m2} \propto E_0 e^{i(-2\pi f_1 t + \varphi_0 + \phi_2)} \\ E_{r2} \propto E_0 e^{i(-2\pi f_2 t + \varphi'_0)} \end{cases}, \quad (3)$$

where E_{m1} and E_{m2} are the electrical fields of measurement beam 1 and measurement beam 2, E_{r1} and E_{r2} are the electrical fields of reference beam 1 and reference beam 2, and ϕ_1 and ϕ_2 are phase changes caused by grating shifting.

The interference signals detected by the R_1 and R_2 are

$$I_1 = |E_{m1} + E_{r1}|^2 \propto \cos(2\pi \Delta f t + \Delta\phi + \phi_1), \quad (4)$$

$$I_2 = |E_{m2} + E_{r2}|^2 \propto \cos(2\pi \Delta f t + \Delta\phi + \phi_2), \quad (5)$$

where I_1 is the interference signal detected by R_1 , and I_2 is the interference signal detected by R_2 ; Δf is $f_1 - f_2$, and $\Delta\phi$ is $\varphi_0 - \varphi'_0$.

When the grating moves, the phase changes ϕ_1 , and ϕ_2 can be extracted. According to the Doppler shift, the phase changes ϕ_1 and ϕ_2 can be expressed as

$$\phi_1 = \frac{4\pi \sin \theta}{\lambda} \Delta x + \frac{4\pi \cos \theta}{\lambda} \Delta z, \quad (6)$$

$$\phi_2 = -\frac{4\pi \sin \theta}{\lambda} \Delta x + \frac{4\pi \cos \theta}{\lambda} \Delta z, \quad (7)$$

where θ is the Littrow angle, λ is the wavelength of the laser, Δx is the displacement along the x axis, and Δz is the displacement along the z axis.

From Eqs. (6) and (7) and the grating equation $2d \sin \theta = m\lambda$ ($m = 1, 2, 3, \dots$), the displacement of the grating in x and z directions can be written as follows:

$$\Delta x = \frac{d}{4\pi m} (\phi_1 - \phi_2), \quad (8)$$

$$\Delta z = (\phi_1 + \phi_2) \frac{d}{4\pi m \cot \theta}, \quad (9)$$

where d is the grating period.

The readings of the system after subdivision are given by

$$\phi_1 = k_1 \frac{2\pi}{N}, \quad (10)$$

$$\phi_2 = k_2 \frac{2\pi}{N}, \quad (11)$$

where k_1 and k_2 are the readings of the system after subdivision, and N is the multiplier of the electronic subdivision.

Then the displacements in x and z directions can be written as follows:

$$\Delta x = \frac{d}{2mN} (k_1 - k_2), \quad (12)$$

$$\Delta z = \frac{d}{2mN \cot \theta} (k_1 + k_2). \quad (13)$$

It can be seen from Eqs. (12) and (13) that the resolution of the system is $d/(2mN)$ in the x direction and $d/(2mN \cot \theta)$ in the z direction.

3. SYSTEM PERFORMANCE TEST

A. Experimental Setup

To test the performance of the two-dimensional grating-based interferometer, we designed an experiment to compare our proposed interferometer with the dual-frequency laser interferometer. Figure 2 is a schematic diagram of the experimental configuration. An He-Ne laser ($\lambda = 632.8$ nm) was used as the light source. The beam was divided into three paths by the beam splitters (BS_1 and BS_2) and mirrors ($M_1 - M_3$). One of the beams entered the reading head of the grating-based interferometer, and the other two entered the two dual-frequency laser interferometers LI_1 and LI_2 (10706B, KEYSIGHT). M_4 , M_5 , and the one-dimensional grating were fixed on a precision linear stage (PLS) (Q-545, Physik Instrumente). The range of the PLS was 13 mm. The grating was made by our laboratory with a size of 50 mm \times 25 mm \times 6 mm and a period of 555.56 nm. The blaze angle was 40.4 degrees, and the diffraction efficiency was about 65% at 632.8 nm. On one hand, the reason for using this grating is that it can improve optical resolution. On the other hand, the incident angle is favorable for installation. LI_1 and M_4 were

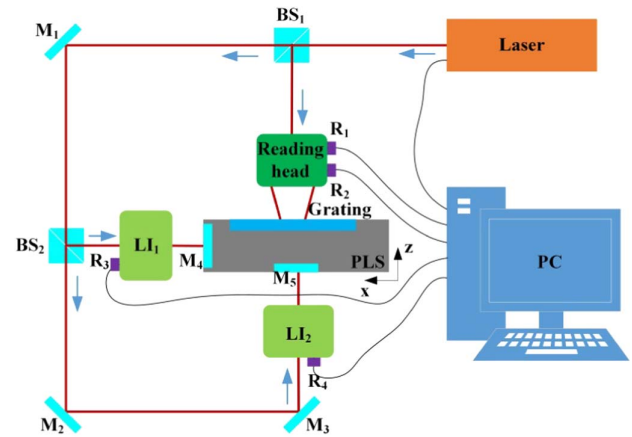


Fig. 2. Schematic diagram of the experimental configuration.

used to measure displacement of the PLS in the x direction, while LI_2 and M_5 were used to measure displacement in the z direction. Receivers R_1 and R_2 were responsible for receiving interference signals from the two-dimensional grating-based interferometer. Receivers R_3 and R_4 received the interference signals from LI_1 and LI_2 , respectively. $R_1 - R_4$ (Remote Receiver 10780F, KEYSIGHT) transformed the interference signals into electrical signals and input them to the computer. We then processed the data to obtain the displacement measurement values in x and z directions.

To make the reading head smaller and more compact, we used the two PBS modules, shown in Figs. 3 and 4, which integrated a PBS, two QW plates, and a mirror to replace PBS_1 and PBS_2 , $QW_1 - QW_4$, and M_2 and M_4 in Fig. 2. This greatly reduced the size and complexity involved in adjusting the system. Because the PLS was a one-dimensional linear displacement stage, the displacements in x and z directions needed to be measured separately in the actual experiment. The actual optical path diagrams are shown in Figs. 3 and 4. In the two figures, the solid red line represents the propagation path of the laser. Figure 3 shows the experimental setup for measuring the displacement in the x direction. The laser was split into two beams by a BS (BS_1). One beam was reflected into the

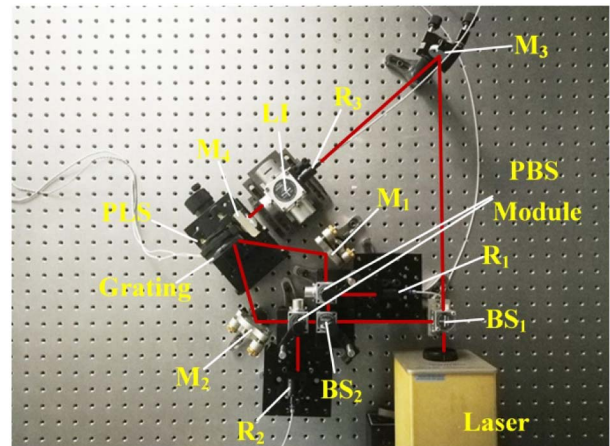


Fig. 3. Experimental setup for displacement measurements in the x direction.

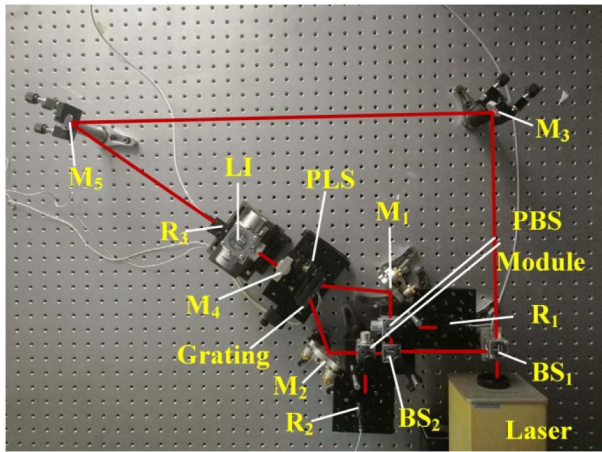


Fig. 4. Experimental setup for displacement measurements in the z direction.

dual-frequency laser interferometer by a mirror (M_3). The other directly entered the reading head of the grating-based interferometer. The reading head contained only a BS (BS_2), two PBS modules, and two mirrors (M_1 and M_2). The grating was fixed on a three-dimensional adjustable frame that was installed on the displacement stage. The vector direction of the grating was parallel to the direction of motion of the PLS. The surface of the mirror (M_4) was perpendicular to the grating's surface. Figure 4 shows the experimental setup for measuring displacement in the z direction. Unlike in Fig. 3, in Fig. 4, the vector direction of the grating is perpendicular to the direction of motion of the PLS. The surface of the mirror (M_4) was parallel to the grating. To reduce the influence of ambient changes in temperature, air flow, and other mechanical vibration, the whole experimental device was built on an air floatation stage that was placed in the laboratory's inner workroom (a closed working space built inside the laboratory), and the reading heads of the two systems were covered.

B. Millimeter Range Tests

To demonstrate that the proposed grating-based interferometer was capable of measuring displacement in two directions, we first carried out millimeter range tests in both x and z directions. The range of the PLS was set to 10 mm and the speed to 10 mm/s. Figure 5 shows the displacement measurement results and the difference in the x direction. The legend LI refers to the laser interferometer, and GI refers to the proposed grating-based interferometer. It is worth noticing that both displacements were 10 mm, and the curve obtained using

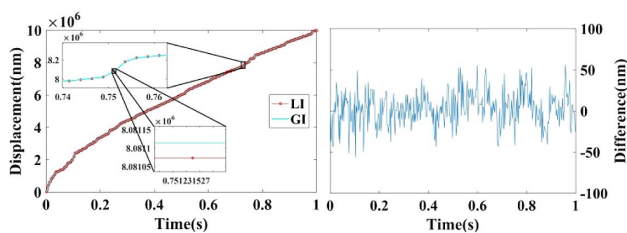


Fig. 5. Measurement results and the difference in the x direction.

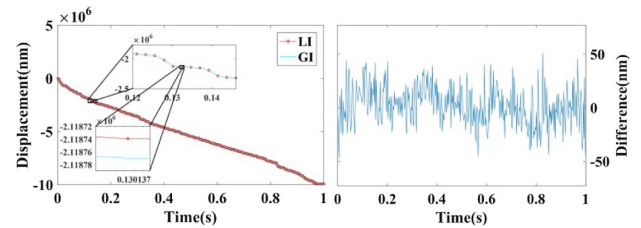


Fig. 6. Measurement results and the difference in the z direction.

our proposed interferometer corresponded closely with the curve obtained with the laser interferometer. The velocity stability of the PLS was not ideal, resulting in slight fluctuations in the displacement curve. However, we were able to detect these unwanted sections with the grating-based interferometer, and they matched the laser interferometer almost perfectly. The graph of the displacement difference shows that it fluctuated around 0. The 3σ values for the difference were 60.19 nm. The discrepancy resulted mainly from grating's surface error and the yaw in the PLS. The surface error (flatness of grating surface) and line error (pitch deviation of grating) of the grating both affect displacement measurement of the system, because the surface error and line error affect the diffraction wave fronts. It then changes the phase of the interference signal. The load capacity of the PLS was limited. The load was unevenly distributed on the displacement stage, which exacerbated the yaw in the PLS. The yaw in the PLS had different effects on the two systems because of the differences in measurement methods. Figure 6 shows displacement measurement results and the difference in the z direction. Measurement results for the two systems corresponded closely. The displacement difference fluctuated around 0. The 3σ values for the difference were 54.12 nm. The discrepancy resulted mainly from the grating's surface error and yaw in the PLS.

C. Micrometer Range Tests

To demonstrate the repeatability of our proposed interferometer, the PLS was driven to produce a displacement of $3\ \mu\text{m}$ in $1\text{-}\mu\text{m}$ steps. The dual-frequency laser interferometer was also used to simultaneously measure the movement of the stage for comparison. The experimental results are shown in Figs. 7 and 8. Figure 7 shows measurement results and the difference in the x direction. As can be seen in Fig. 7, the two displacement curves were in good agreement. The 3σ values for the difference during the movement of the PLS are 10.10 nm, 11.33 nm, and 11.00 nm. The 3σ values for the difference at rest are 2.75 nm, 4.27 nm, 2.92 nm, and 3.46 nm. Figure 8

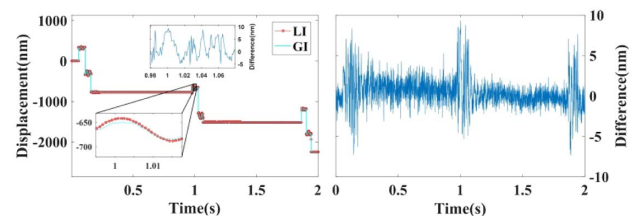


Fig. 7. Measurement results and the difference for a displacement of $3 \times 1\ \mu\text{m}$ in the x direction.

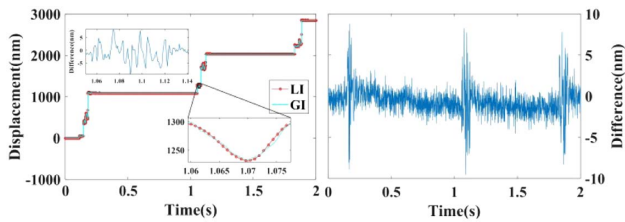


Fig. 8. Measurement results and the difference for a displacement of $3 \times 1 \mu\text{m}$ in the z direction.

shows measurement results and the difference in the z direction. The 3σ values for the difference during the movement are 9.69 nm, 11.21 nm, and 10.80 nm. The 3σ values for the difference at rest are 2.57 nm, 3.36 nm, 3.17 nm, and 4.46 nm. The difference was caused mainly by high-frequency electronic error, environmental changes, and yaw in the PLS. Experimental results show that the repeatability of our interferometer is better than 2 nm in x and z directions.

D. Nanometer Range Tests

The theoretical resolutions of our proposed interferometer in x and z directions were 0.27 nm and 0.18 nm, respectively. To test the resolution of the grating-based interferometer in actual displacement measurements, the PLS was driven to produce a displacement of 9 nm in 3-nm steps. The experimental results are shown in Figs. 9 and 10. Figures 9 and 10 show measurement results and the difference in x and z directions. As can be seen from the figures, the grating-based interferometer had a displacement resolution of 3 nm, and the two displacement curves were in good agreement. The displacement difference fluctuated around 0. The 3σ values for the difference were 1.67 nm in the x direction and 1.35 nm in the z direction. The difference in the displacement measurement was caused

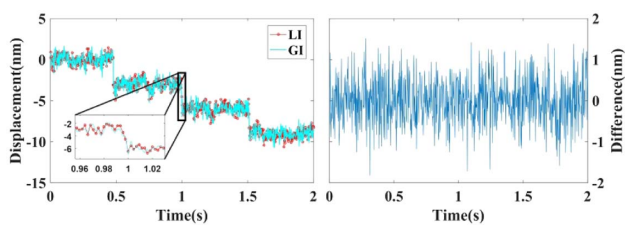


Fig. 9. Measurement results and the difference for a displacement of $3 \times 3 \text{ nm}$ in the x direction.

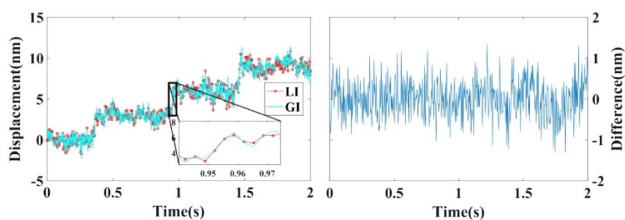


Fig. 10. Measurement results and the difference for a displacement of $3 \times 3 \text{ nm}$ in the z direction.

mainly by high-frequency electronic error and environmental changes. Figure 10 shows that environmental changes cause the curves of the two systems to fluctuate when at rest, which limits the system resolution. The minimum step for our PLS was 3 nm. However, the results demonstrated that our proposed interferometer has the potential to resolve smaller displacements.

E. Stability Tests

To demonstrate the stability of our system, the stage was held stationary, and the displacement was measured within 5 s and 30 min. Figure 11 shows the measurement results for stability tests within 5 s in x and z directions. The figure shows that high-frequency noise, environmental vibration, and the vibration prevent the curves of the two systems from being ideal straight lines. The displacement for both systems fluctuated around 0. The 3σ values for the grating interferometer were 1.73 nm in the x direction and 2.24 nm in the z direction. Figure 12 shows measurement results for stability tests within 30 min in x and z directions. As we can see in Fig. 12, the stability of our system in both x and z directions is better than that of the laser interferometer.

The above measurement results demonstrate that our proposed interferometer can carry out from nanometer to millimeter displacement measurements with high precision in both x and z directions. The system also showed good repeatability and stability. We set up a reading head consisting of a BS, two PBS modules, and two mirrors, which was very simple and compact. In addition, three-dimensional displacement measurements can be carried out with the two-dimensional grating by replacing the beam prism with a two-dimensional grating and adding two identical PBS modules and mirrors, extending the application range while keeping the size of the reading head small.

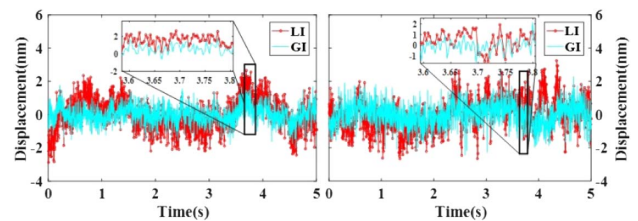


Fig. 11. Measurement results for stability tests within 5 s in the x direction (left) and z direction (right).

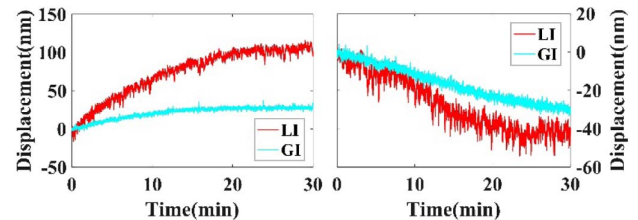


Fig. 12. Measurement results for stability tests within 30 min in the x direction (left) and z direction (right).

4. DISCUSSION

The yaw between the reading head, grating, and displacement stage has a significant impact on measurement accuracy of the grating-based interferometer. An analysis of the influence of the yaw angle on displacement measurements will assist in improving measurement accuracy of the system, as shown in detail below.

A. Case 1: Yaw Angle (α) Between the Grating and the Displacement Stage

In Fig. 13, there is no yaw angle between the grating and the reading head, but a yaw angle (α) occurs between the grating and the displacement stage. When the displacement stage moves in the x direction a distance of Δx , the displacement of the system in the vector direction of the grating is given by

$$\Delta x' = \Delta x \cos \alpha, \tag{14}$$

where $\Delta x'$ represents displacement of the system in the vector direction of the grating.

Displacement of the system in the direction normal to the grating is given by

$$\Delta z' = \Delta x \sin \alpha, \tag{15}$$

where $\Delta z'$ is displacement of the system in the direction normal to the grating.

Measurement errors of the grating-based interferometer in x and z directions are given by

$$\Delta x_{\text{error}} = \Delta x(1 - \cos \alpha), \tag{16}$$

$$\Delta z_{\text{error}} = \Delta x \sin \alpha, \tag{17}$$

where Δx_{error} is the measurement error of the grating-based interferometer in the x direction, and Δz_{error} is the measurement error in the z direction.

Similarly, when the displacement stage moves in the z direction a distance of Δz , measurement errors of the grating-based interferometer in x and z directions are given by

$$\Delta x_{\text{error}} = \Delta z \sin \alpha, \tag{18}$$

$$\Delta z_{\text{error}} = \Delta z(1 - \cos \alpha). \tag{19}$$

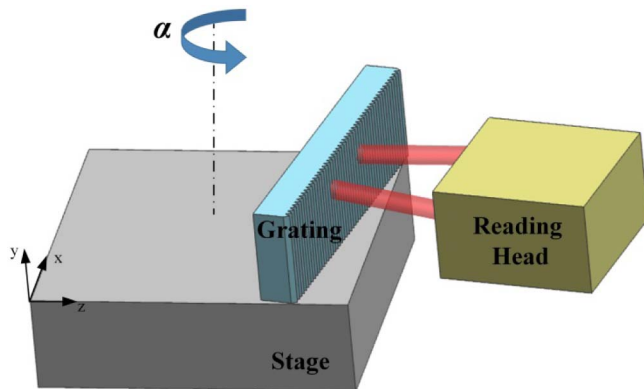


Fig. 13. Sketch of yaw angle between the grating and the displacement stage.

This case will introduce cosine errors to the system in both directions. Measurement errors increase with an increase in the yaw angle, which significantly affects the accuracy of displacement measurement. But the errors will be linear, which makes them easier to find and reduce.

B. Case 2: Yaw Angle (β) Between the Grating and the Reading Head

In Fig. 14, there is no yaw angle between the grating and the displacement stage, but a yaw angle (β) occurs between the grating and the reading head. Because the yaw angle is very small, differentiating both sides of the grating equation $d(\sin \theta_i + \sin \theta_q) = m\lambda$ will give

$$\cos \theta_i d\theta_i + \cos \theta_q d\theta_q = 0, \tag{20}$$

where θ_i is the angle of incidence, and θ_q is the angle of diffraction.

In the Littrow configuration, $\theta_i = \theta_q$, and so Eq. (20) can be written as

$$d\theta_i = -d\theta_q. \tag{21}$$

Therefore, the incident beam and the diffracted beam no longer coincide. The absolute value of the variation in the angle of diffraction is the same as the angle of incidence. Equations (6) and (7) can be written as

$$\begin{aligned} \phi'_1 &= \frac{2\pi}{\lambda} [\sin(\theta + \beta) + \sin(\theta - \beta)] \Delta x \\ &+ \frac{2\pi}{\lambda} [\cos(\theta + \beta) + \cos(\theta - \beta)] \Delta z, \end{aligned} \tag{22}$$

$$\begin{aligned} \phi'_2 &= -\frac{2\pi}{\lambda} [\sin(\theta - \beta) + \sin(\theta + \beta)] \Delta x \\ &+ \frac{2\pi}{\lambda} [\cos(\theta - \beta) + \cos(\theta + \beta)] \Delta z. \end{aligned} \tag{23}$$

After simplification, measurement errors of the grating-based interferometer in x and z directions are given by

$$\Delta x_{\text{error}} = \Delta x - \frac{d}{4\pi} (\phi'_1 - \phi'_2) = \Delta x(1 - \cos \beta), \tag{24}$$

$$\Delta z_{\text{error}} = \Delta z - \frac{d}{4\pi \cot \theta} (\phi'_1 + \phi'_2) = \Delta z(1 - \cos \beta). \tag{25}$$

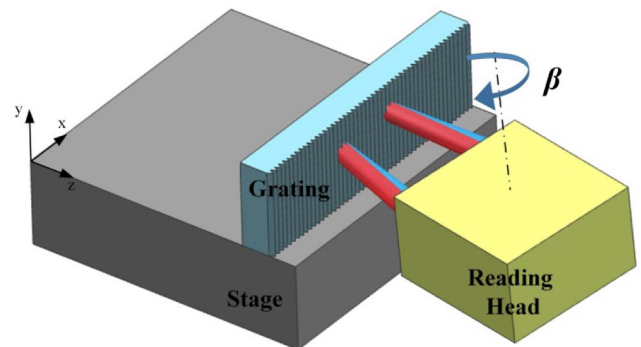


Fig. 14. Sketch of yaw angle between the grating and the reading head.

This case also will introduce cosine errors to the system in both directions. Measurement error increases with an increase in the yaw angle, which affects the accuracy of displacement measurement. However, when there is an angle between the diffracted beam and the incident beam, the spots of the two beams will be separated on the detector. If the angle increases to a critical value, the interference field cannot be detected, so the system cannot measure displacement. The beam diameter of the laser in our experiment is 3 mm. In the worst case, the two spots are completely separated, i.e., the distance between them is 3 mm. Because the receiver used in this experiment employs an optical fiber of a length of 2 mm, the angle between the diffracted beam and the reference beam is about 1.5 mrad. At this magnitude, if the grating moves 1 mm, the difference between the ideal value and the measured value is about 1 nm. In this case, the error can be ignored.

C. Case 3: Yaw Angle (γ) Between the Grating and the Reading Head Because of Yaw in the Stage

The above two cases assume an ideal linear displacement stage. In fact, there will be yaw in the movement of the displacement stage, which will result in displacement measurement errors. Figure 15 is a schematic diagram of the yaw angle (γ) between the reading head and the grating caused by yaw in the stage. The ideal position of the grating is on the x axis. Two beams are incident on points A and B on the grating's plane in the Littrow configuration. When there is a yaw angle (γ) between the grating and the reading head, the actual position of the grating moves from the x axis to the green dotted line ON. Point O is the position of the axis of rotation. The incident points of the two beams also move to points A' and B', through which two straight lines (l_1 and l_2) parallel to the x axis have been drawn in the figure. These two lines intersect the lines drawn normal to the grating at points P and Q. As can be seen in Fig. 15, any rotation in the grating has two effects on the two incident beams. The first is that the grating moves from the x axis in the z direction to positions l_1 and l_2 , respectively. The second is that the grating rotates by an angle γ at points A' and B', respectively. These two effects result in the change in the optical path. Calculation shows that the change in the optical path caused by a rotation of the grating is much less than the change caused by a translation of the grating, and can thus be ignored. From this, the effect of yaw in the grating on the system can be treated as the two incident beams on the grating translating to different positions by distances equal to the lengths of line segments AP and BQ.

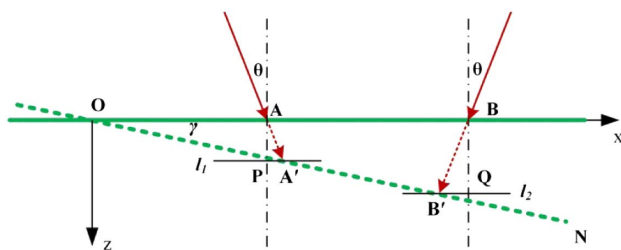


Fig. 15. Schematic diagram of yaw angle (γ) between the reading head and the grating.

The lengths of line segments AP and BQ are given by

$$l_{AP} = \frac{l_{OA} \sin \gamma \cos \theta}{\cos(\theta + \gamma)}, \tag{26}$$

$$l_{BQ} = \frac{(l_{OA} + l_{AB}) \sin \gamma \cos \theta}{\cos(\theta - \gamma)}, \tag{27}$$

where l_{OA} and l_{AB} are the lengths of line segments OA and AB, and l_{AB} is the distance between the two light spots.

Equations (6) and (7) can be written as

$$\phi_1'' = \frac{4\pi \sin \theta}{\lambda} \Delta x + \frac{4\pi \cos \theta}{\lambda} \Delta z + \frac{4\pi \cos \theta}{\lambda} l_{AP}, \tag{28}$$

$$\phi_2'' = -\frac{4\pi \sin \theta}{\lambda} \Delta x + \frac{4\pi \cos \theta}{\lambda} \Delta z + \frac{4\pi \cos \theta}{\lambda} l_{BQ}. \tag{29}$$

When the angle γ is very small, after simplification, displacement measurement errors in the x and z directions can be expressed as

$$\Delta x_{\text{error}} = \frac{l_{AP} - l_{BQ}}{2 \tan \theta} \approx \frac{l_{AB}\gamma}{2 \tan \theta}, \tag{30}$$

$$\Delta z_{\text{error}} = \frac{l_{AP} + l_{BQ}}{2} \approx \left(l_{OA} + \frac{l_{AB}}{2} \right) \gamma. \tag{31}$$

Equations (30) and (31) indicate that the displacement measurement error in the x direction caused by yaw in the displacement stage is related to the distance between the two spots, the yaw angle, and the Littrow angle, and the displacement measurement error in the z direction is related to the distance between the two spots, the yaw angle, and the position of the axis of rotation. If the yaw angle is 10 μ rad and the distance between the two spots is 6 mm, the error in the x direction is about 40 nm. This will significantly affect the accuracy of the displacement measurement. To improve the accuracy of the system, we can use a displacement stage with higher accuracy, reduce the distance between the two spots, and use a grating with a higher line density. If the axis of rotation is located at the center of the two spots, the error in the z direction is close to 0. Although superposition of the two spots will minimize the errors in both x and z directions, it will lead to polarization and frequency mixing errors caused by zero-order diffraction light. For this reason, it is important to keep the two light spots separated by a certain distance.

In the above analyses, the errors we have discussed are linear errors. Since the grating-based interferometer we proposed is a heterodyne interferometer measurement system, there will be nonlinear errors in the system. Nonlinear errors in a grating-based interferometer can be manifested in periodic and nonperiodic nonlinear errors. On one hand, similar to the heterodyne laser interferometer, the periodic nonlinear errors are caused mainly by nonorthogonality and ellipticity of the laser source and misalignment and imperfections of the polarizing optical elements [22,23], because the dual frequency laser and polarizing optical elements are used in the grating-based interferometer. The laser and polarizing elements used in the experiment are provided by Agilent. By checking the instructions, we can learn that the nonlinear error of this part is less than 4.2 nm. On the other hand, unlike the laser interferometer, there is a grating as a ruler in the grating-based

interferometer. The diffraction efficiency of p -polarized light and s -polarized light will be different because of the polarization characteristic of the grating. It will also cause frequency mixing and polarization mixing, which leads to periodic nonlinear errors. The nonperiodic nonlinear error is caused mainly by the surface error and line error of the grating [24]. The quality of the diffraction wavefront is directly affected by the surface and grooves of the grating [25,26]. If there are random errors in the surface and grooves, it will introduce the error phases to the signal, which causes nonperiodic nonlinear error. Because the grating used in the experiment is not very ideal, the nonlinear errors caused by the grating would be greater than those caused by polarizing optical elements and lasers, especially the nonperiodic nonlinear error caused by the grating surface error and line error. It would account for a large proportion of nonlinear errors. Our next work will focus on analyses of the contribution of the grating's diffraction efficiency, polarization characteristics, surface quality, and groove quality to the nonlinear errors of the grating interferometer and method to reduce and compensate the errors, which will further improve accuracy of the system.

5. CONCLUSION

In this study we propose a simple and compact reading head for a two-dimensional grating-based interferometer. The system uses a high-density grating to achieve high resolution, heterodyne to achieve high accuracy and stability, Littrow configuration to achieve 2D displacement measurement and a simple structure. The reading head contains a BS, two PBS modules, and two mirrors. The grating-based interferometer can measure the displacement in both x and z directions with theoretical resolutions of 0.27 nm and 0.18 nm, respectively. We carried out several experiments to compare the feasibility and performance of the proposed interferometer with the dual-frequency laser interferometer. The results show that our interferometer can measure displacements from 3 nm to 10 mm with high accuracy. The system also has good repeatability and stability. The 3σ values for the difference are 1.67 nm in the x direction and 1.35 nm in the z direction for a displacement of 9 nm. Repeatability of our interferometer for a displacement of 1 μm is better than 2 nm. We also analyzed the errors caused by yaw angles between the grating, reading head, and displacement stage and proposed methods to reduce these errors. With the proposed structure, the reading head can be easily integrated further by using smaller optical elements, which will produce a grating-based interferometer that is easy to install and that can be used in a wider range of applications. This simple structure is also easy to extend for three-dimensional displacement measurements. This grating-based interferometer with its simple structure, small size, and easy installation should play an important role in the field of precision measurement. In future work, we will integrate the various parts of the reading head and analyze influences of grating errors on measurement to further improve accuracy of the system.

Funding. National Natural Science Foundation of China (NSFC) (61227901, 61741517); Jilin Province Science & Technology Development Program Project in China

(20180201035GX); Jilin Province Special Funds for High-tech Industrialization in cooperation with the Chinese Academy of Sciences (CAS) (2018SYHZ0014).

REFERENCES

1. M. Malinauskas, A. Zukauskas, S. Hasegawa, Y. Hayasaki, V. Mizeikis, R. Buividas, and S. Juodkakis, "Ultrafast laser processing of materials: from science to industry," *Light Sci. Appl.* **5**, e16133 (2016).
2. A. C. Urness, M. C. Cole, K. K. Kamysiak, E. R. Moore, and R. R. McLeod, "Liquid deposition photolithography for submicrometer resolution three-dimensional index structuring with large throughput," *Light Sci. Appl.* **2**, e56 (2013).
3. K. Sugioka and Y. Cheng, "Ultrafast lasers—reliable tools for advanced materials processing," *Light Sci. Appl.* **3**, e149 (2014).
4. S. M. Jing, X. Y. Zhang, J. F. Liang, C. Chen, Z. M. Zheng, and Y. S. Yu, "Ultrashort fiber Bragg grating written by femtosecond laser and its sensing characteristics," *Chin. Opt.* **10**, 449–454 (2017).
5. B. G. Chen, M. Ming, and T. Y. Lv, "Precise measurement of curvature radius for spherical mirror with large aperture," *Chin. Opt.* **7**, 163–168 (2014).
6. E. Z. Zhang, B. Y. Chen, H. Zheng, L. Yan, and X. Y. Teng, "Laser heterodyne interferometer with rotational error compensation for precision displacement measurement," *Opt. Express* **26**, 90–98 (2018).
7. Y. T. Lou, L. P. Yan, B. Y. Chen, and S. H. Zhang, "Laser homodyne straightness interferometer with simultaneous measurement of six degrees of freedom motion errors for precision linear stage metrology," *Opt. Express* **25**, 6805–6821 (2017).
8. Q. Lv, W. H. Li, Bayanheshig, Y. Bai, Z. W. Liu, and W. Wang, "Interferometric precision displacement measurement system based on diffraction grating," *Chin. Opt.* **10**, 39–50 (2017).
9. W. T. Estler, "High-accuracy displacement interferometry in air," *Appl. Opt.* **24**, 808–815 (1985).
10. F. M. Gerasimov, "Use of diffraction gratings for controlling of a ruling engine," *Appl. Opt.* **6**, 1861–1865 (1967).
11. D. H. Mollenhauer, P. Ijju, and B. Han, "A compact, robust, and versatile moiré interferometer," *Opt. Lasers Eng.* **23**, 29–40 (1995).
12. Y. C. Chung, K. C. Fan, and B. C. Lee, "Development of a novel planar encoder for 2D displacement measurement in nanometer resolution and accuracy," in *Proceedings of IEEE Conference on Intelligent Control and Automation* (IEEE, 2011), pp. 449–453.
13. H. L. Hsieh, J. C. Chen, G. Lerondel, and J. Y. Lee, "Two-dimensional displacement measurement by quasi-common-optical-path heterodyne grating interferometer," *Opt. Express* **19**, 9770–9782 (2011).
14. X. Li, W. Gao, H. Muto, Y. Shimizu, S. Ito, and S. Dian, "A six-degree-of-freedom surface encoder for precision positioning of a planar motion stage," *Precis. Eng.* **37**, 771–781 (2013).
15. W. Gao and A. Kimura, "A three-axis displacement sensor with nanometric resolution," *CIRP Ann.* **56**, 529–532 (2007).
16. H. L. Hsieh and S. W. Pan, "Development of a grating-based interferometer for six-degree-of-freedom displacement and angle measurements," *Opt. Express* **23**, 2451–2465 (2015).
17. H. L. Hsieh and S. W. Pan, "Three-degree-of-freedom displacement measurement using grating-based heterodyne interferometry," *Appl. Opt.* **52**, 6840–6848 (2013).
18. J. Guan, P. Kochert, C. Weichert, and R. Tutsch, "A high performance one-dimensional homodyne encoder and the proof of principle of a novel two-dimensional homodyne encoder," *Precis. Eng.* **37**, 865–870 (2013).
19. W. Trutna, Jr., G. Owen, A. Ray, J. Prince, E. Johnstone, M. Zhu, and L. Cutler, "Littrow interferometer," US Grant US7440113 (21 October 2008).
20. Y. Lu, C. Wei, W. Jia, S. B. Li, J. J. Yu, M. K. Li, C. C. Xiang, X. S. Xiang, J. Wang, J. Y. Ma, and C. H. Zhou, "Two degree-freedom displacement measurement based on a short period grating in symmetric Littrow configuration," *Opt. Commun.* **380**, 382–386 (2016).
21. L. Šiaudinytė, G. Molnar, R. Köning, and J. Flügge, "Multi-dimensional grating interferometer based on fibre-fed measurement heads

- arranged in Littrow configuration," *Meas. Sci. Technol.* **29**, 054007 (2018).
22. C. M. Wu and C. S. Su, "Nonlinearity in measurements of length by optical interferometry," *Meas. Sci. Technol.* **7**, 62–68 (1996).
 23. C. M. Wu, J. Lawall, and R. D. Deslattes, "Heterodyne interferometer with subatomic periodic nonlinearity," *Appl. Opt.* **38**, 4089–4094 (1999).
 24. X. Xing, D. Chang, P. C. Hu, and J. B. Tan, "Spatially separated heterodyne grating interferometer for eliminating periodic nonlinear errors," *Opt. Express* **25**, 31384–31393 (2017).
 25. S. Yokozeki and S. Sawa, "Interferometric testing of grating using moire method," *Jpn. J. Appl. Phys.* **14**, 465–470 (1975).
 26. Z. Jaroszewicz, "Interferometric testing of the spacing error of a plane diffraction grating," *Opt. Commun.* **60**, 345–349 (1986).